

**Tailoring Crystallinity of BiVO<sub>4</sub> Films for Water Splitting by Pulsed Laser Deposition**

by

**Chu-Yu Cheng**

B.S., National Tsing Hua University, 2018

Submitted to the Graduate Faculty of  
Swanson School of Engineering in partial fulfillment  
of the requirements for the degree of  
Master of Science

University of Pittsburgh

2021

UNIVERSITY OF PITTSBURGH

SWANSON SCHOOL OF ENGINEERING

This thesis was presented

by

**Chu-Yu Cheng**

It was defended on

March 29, 2021

and approved by

Jung-Kun Lee, PhD, Professor

Department of Mechanical Engineering and Material Science

Jörg Wiezorek, PhD, Professor

Department of Mechanical Engineering and Material Science

Wissam Abdo Saidi, PhD, Associate Professor

Department of Mechanical Engineering and Material Science

Thesis Advisor:

Jung-Kun Lee, PhD, Professor

Department of Mechanical Engineering and Material Science

Copyright © by Chu-Yu Cheng

2021

# **Tailoring Crystallinity of BiVO<sub>4</sub> Films for Water Splitting by Pulsed Laser Deposition**

Chu-Yu Cheng, M.S.

University of Pittsburgh, 2021

Bismuth vanadate (BiVO<sub>4</sub>) is one of the most popular candidates among materials for solar water splitting. In previous studies, typical BiVO<sub>4</sub> films exhibit limitations due to poor charge carrier mobility. Recently, it has been reported that this drawback could be fixed with synthesis of BiVO<sub>4</sub> films via pulsed laser deposition. In this thesis, the effect of temperature and substrate on the microstructure of BiVO<sub>4</sub> films is studied. The thickness and crystallographic orientation could be controlled by executing the deposition under different conditions. BiVO<sub>4</sub> films deposited at temperature higher than 500°C demonstrate gradual change in crystallographic orientation as temperature increases, showing certain level of preferred orientation comparing with those synthesized under room temperature. In addition, the films with higher tendency of preferred orientation also show higher photocurrent density during photoelectrochemical characterization.

## Table of Contents

Nomenclature .....	ix
Acknowledgement.....	x
<b>1.0 Introduction.....</b>	<b>1</b>
<b>2.0 Background Information and Theory.....</b>	<b>5</b>
<b>2.1 Fundamentals of Hydrogen Evolution Reaction .....</b>	<b>5</b>
<b>2.2 Photoelectrochemical Cells (PEC) .....</b>	<b>8</b>
<b>2.3 Material Requirements for Photoanodes .....</b>	<b>9</b>
<b>2.3.1 Energy Band Theory.....</b>	<b>10</b>
<b>2.3.2 Catalytic Activity and Stability.....</b>	<b>12</b>
<b>2.3.3 Charge Carrier Mobility .....</b>	<b>13</b>
<b>2.4 Bismuth Vanadate .....</b>	<b>14</b>
<b>2.4.1 Properties of Bismuth Vanadate.....</b>	<b>14</b>
<b>2.4.2 Synthesis of Bismuth Vanadate .....</b>	<b>17</b>
<b>2.5 Crystallographic Orientation .....</b>	<b>18</b>
<b>2.6 Pulsed Laser Deposition (PLD) .....</b>	<b>20</b>
<b>2.6.1 Introduction for PLD.....</b>	<b>20</b>
<b>2.6.2 Basic Concept of PLD.....</b>	<b>21</b>
<b>2.6.3 Influence of Deposition Condition .....</b>	<b>23</b>
<b>3.0 Research Description .....</b>	<b>24</b>
<b>3.1 Hypothesis .....</b>	<b>24</b>
<b>3.2 Objectives .....</b>	<b>24</b>

<b>3.3 Research Tasks .....</b>	<b>25</b>
<b>4.0 Experimental Section.....</b>	<b>26</b>
<b>4.1 Synthesis of BiVO<sub>4</sub> Films with PLD.....</b>	<b>26</b>
<b>4.2 Microstructural Characterization .....</b>	<b>27</b>
<b>4.3 Electrochemical Characterization .....</b>	<b>27</b>
<b>5.0 Experimental Results and Discussion .....</b>	<b>30</b>
<b>5.1 Thickness Control of BiVO<sub>4</sub> Films.....</b>	<b>30</b>
<b>5.1.1 Growth Behavior as a function of Oxygen Partial Pressure .....</b>	<b>31</b>
<b>5.1.2 Thickness as a function of repetition rate and deposition time.....</b>	<b>32</b>
<b>5.2 Microstructure of BiVO<sub>4</sub> Films.....</b>	<b>34</b>
<b>5.3 PEC Performance of BiVO<sub>4</sub> Films.....</b>	<b>37</b>
<b>5.3.1 Influence of Temperature to PEC Performance .....</b>	<b>38</b>
<b>5.3.2 Influence of Thickness to PEC Performance of BiVO<sub>4</sub> Films.....</b>	<b>39</b>
<b>5.4 Future Work .....</b>	<b>41</b>
<b>6.0 Conclusion .....</b>	<b>44</b>
<b>Bibliography .....</b>	<b>46</b>

## List of Tables

<b>Table 1 Film thickness and appearance under different oxygen partial pressure .....</b>	<b>31</b>
<b>Table 2 Film thickness under various deposition conditions .....</b>	<b>33</b>

## List of Figures

<b>Figure 1 Structure of a PEC cell.....</b>	<b>9</b>
<b>Figure 2 Band distribution of common semiconductors .....</b>	<b>11</b>
<b>Figure 3 Carrier mobility of common semiconductors .....</b>	<b>13</b>
<b>Figure 4 Random orientation vs. preferred orientation .....</b>	<b>19</b>
<b>Figure 5 Experimental setup of a PLD system [14] .....</b>	<b>21</b>
<b>Figure 6 Electrode setup for photoelectrochemical measurements. ....</b>	<b>28</b>
<b>Figure 7 Physical Appearance of films deposited under (a) No Oxygen (b) 5mtorr (c) 10 mtorr .....</b>	<b>32</b>
<b>Figure 8 SEM images of BiVO<sub>4</sub> Films.....</b>	<b>35</b>
<b>Figure 9 XRD plots of BiVO<sub>4</sub> Films .....</b>	<b>36</b>
<b>Figure 10 J-V curves of BiVO<sub>4</sub> films with thickness of 600nm with different repetition rate. (a)40Hz , 20minutes (b) 15Hz, 120minutes .....</b>	<b>38</b>
<b>Figure 11 Photocurrent density of 600°C deposited BiVO<sub>4</sub> Films with various thickness ..</b>	<b>40</b>
<b>Figure 12 Schematic diagram of conductive AFM system.....</b>	<b>42</b>
<b>Figure 13 The expected atomic arrangement at the interface .....</b>	<b>43</b>

## Nomenclature

PLD Pulsed laser deposition

FTO Fluorine doped tin oxide

LSV Liner sweep voltammetry

SEM Scanning electron microscope

XRD X-Ray Diffraction

NHE Normal hydrogen electrode

RHE Reversible hydrogen electrode

## **Acknowledgement**

I would like to gratefully give my sincere appreciation to my advisor Dr. Jung-Kun Lee for his patience and guidance in such a difficult period of time. Dr. Lee not only supported me academically, but also emotionally supported me to make better decisions in my life. I wouldn't have accomplished my research without his knowledge and generosity.

I sincerely appreciate my committee members: Prof. Jörg Wiezorek, Prof. Wissam Saidi, and Prof. Jung-Kun Lee for their time to help improve this thesis.

I also want to thank other members in my research group: Dr. Salim Caliskan, Seongha Lee, Sumin Bae, Anqi Wang, Yulin Liu and Joseph Damian. Their support made the process of this thesis smoother.

I would also thank Dr. James Greer and Matthew France for insightful knowledge and technical support.

Finally, I would like to thank my family for their support during the time.

## 1.0 Introduction

The consumption of energy has increased over decades due to the rapid development of high energy consuming technologies. According to the Global Energy Review, the demand for energy worldwide rose by 2.3% in 2018, which is the biggest this decade. The primary energy source human relies on is fossil fuel. It has only been 200 years since we started to consume fossil fuels while it took millions of years to form the fuels. There is no universal agreement of an exact period when we would run out of fossil fuels, but the estimation generally states that fossil fuels would be depleted by 2060 if the rate of consumption remains at the same level. As a result, the crisis of energy shortage has risen in recent years. Meanwhile, global warming has drawn attention simultaneously with energy shortage. Global warming is the long-term heating of the Earth due to human activities especially the combustion of fossil fuels. The rising temperature could lead to ice loss in the pole, rise of sea levels, and result in severe changes in weather and biodiversity.

Thus, research in clean energy source has been widely studied in recent decades. Sources like tides, wind, and geothermal energy are converted into energy all over the globe. However, the sources suffer from regional and seasonal restrictions, making these renewable energies unstable. In order to avoid these limitations, the technique of obtaining hydrogen from water splitting is under development intensively.

There are several known methods of water splitting. Water splitting is the chemical reaction that water is being decomposed into hydrogen and oxygen. A method that splits water both efficiently and economically would be crucial leading to a hydrogen based economy system in the future. Various techniques for water splitting have been

classified into two prominent paths throughout the years. Electrochemical route and photoelectrochemical route are the main categories of water splitting. The electrochemical route is to decompose water into hydrogen and oxygen by letting current pass through water. On the other hand, the photoelectrochemical path, also known as solar path, hydrogen is produced from water using solar illumination and suitable photocatalyst. Among the techniques people have done, water splitting via photocatalytic and photoelectrochemical route has drawn high attention since the solar energy could be used directly during the process. Solar energy has the highest supply capacity among the renewable energy sources. In fact, the energy withing the incident sunlight reaching the earth every hour meets the total energy demand of the world.

Metal oxide semiconductors are materials offering possibilities for wide applications. Oxide semiconductors are advantageous in several ways. The wide band gap of oxide semiconductors offers the durability of temperature during its operation. The rising temperature has far less effect on the device's functionality. In addition, the wide band gap also allows oxide semiconductor materials to handle higher voltages and power. The ability to stay functional in difficult situations make oxide materials important among the semiconductors.

Numerous researches about photocatalytic have been conducted. Hence, the diversity of materials selection is tremendous. Several oxide semiconductors are known to behave as photoanode on which oxygen evolution occurs. Among the semiconducting materials, monoclinic bismuth vanadate ( $\text{BiVO}_4$ ) has been one of the top materials people have had high interest in because  $\text{BiVO}_4$  meets most of the criteria for making a decent photoelectrochemical (PEC) device.  $\text{BiVO}_4$  is one of the most promising material with

superb visible light absorption and a favorable energy band distribution, more importantly, it demonstrates modest stability in neutral electrolytes. However,  $\text{BiVO}_4$  suffer from drawbacks such as low carrier mobility and small hole collection depth. [1-4] In order to deal with the limitations, research about boosting the properties mentioned of  $\text{BiVO}_4$  has been widely studied. Enhancements such as doping and coating with electrocatalysts have been made. In spite of these efforts, the impact of crystallographic orientation remains incompletely studied. Recently, studies have been conducted indicating that applying pulsed laser deposition can increase the carrier mobility and control the growth orientation of films, and controlling the crystallographic orientation of the films being grown as preferred orientation helps enhancing the overall photoelectrochemical performance. The temperature under which the deposition is done determines the orientation of the  $\text{BiVO}_4$  films. By examining the X-Ray Diffraction peaks, we could interpret whether the films demonstrate preferred orientation towards certain directions with the grains.

This thesis is organized in the following chapters. A brief introduction of  $\text{BiVO}_4$  is demonstrated in chapter 1, followed by the review of hydrogen evolution reactions (HER) and the development of  $\text{BiVO}_4$  photoanodes along with different techniques to synthesize  $\text{BiVO}_4$  films in chapter 2. With an analysis of the advantages and disadvantages of the other techniques fabricating  $\text{BiVO}_4$  films, pulsed laser deposition (PLD) is introduced. The review of pulsed laser deposition is also introduced in this chapter. Chapter 3 shows the hypothesis and the objectives and tasks of experiments of this thesis. Chapter 4 demonstrates the experimental details and setup from materials synthesis and the measurements of photoelectrochemical properties for the  $\text{BiVO}_4$  films. Chapter 5 shows the results and data from the experiments, including the LSV curves and SEM, XRD data

along with the film thickness. Chapter 6 will be the overall conclusion and further works of this thesis.

## 2.0 Background Information and Theory

### 2.1 Fundamentals of Hydrogen Evolution Reaction

The hydrogen evolution reaction (HER) has been under research under decades. HER is classified as a cathodic reaction under water splitting among electrochemical reactions. Electrocatalysis is considered to be serving as one of the most important roles in HER. HER involves the adsorption of hydrogen taking place at the surface of the electrode. In general, adsorption and desorption rates of reactants and products is crucial for the activity of a catalyst. The electron transfer is coupled to the adsorption and desorption of hydrogen at the interface of the electrolyte and the cathode.

Under standard conditions, the Nernst potential where equilibrium is reached for HER using a reference electrode of normal hydrogen electrode (NHE) is shown as below:

$$E_{\text{HER}} = E_{0(\text{H}_2/\text{H}^+)} - \frac{RT}{F} * \ln (a_{\text{H}^+} / P_{\text{H}_2}^{1/2}) = -0.059 * (\text{pH}) \text{ V vs. NHE} = 0\text{V vs. RHE}$$

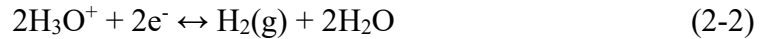
The Nernst potential shows the equilibrium potential where the reaction may occur. Nonetheless, in laboratory environment, the HER scarcely takes place at the equilibrium state. This is reasonable due to the demand of extra activation energy because in most reactions, an activation energy barrier has to be overcome for the HER to proceed. The value of the energy barrier is highly dependent on the nature of the interface where the reaction takes place. HER doesn't initiate until a cathodic potential that is sufficient to drive the reaction is applied. The potential to drive HER could be calculated as below:

$$E_i = E_{\text{HER}} + iR + \eta \quad (2-1)$$

$iR$  is considered the ohmic potential decrease due to the current flow in the electrolyte while  $\eta$  is the reaction overpotential. The overpotential is the most crucial parameters for evaluating the device's performance. When the overpotential is low, the overall efficiency becomes high. In order to enhance the efficiency of the HER reaction, catalysts are often applied to decrease the overpotential so the HER reaction could initiate with a relatively lower driving force. Generally speaking, a decent HER catalyst should be able to lower the overpotential to less than 100mV.

The HER reaction formula is different in acidic environment and alkaline environments as shown below:

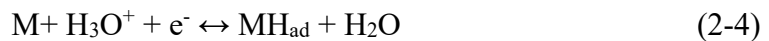
In acidic solution;



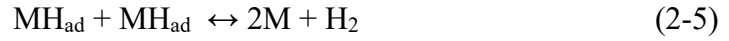
In base solution;



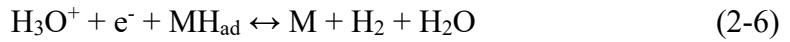
During the initial step, a proton and an electron forms an adsorbed hydrogen atom  $\text{H}_{\text{ad}}$  on the surface of the cathode (M). This step is called Volmer reaction.



The hydrogen desorption could proceed through two different pathways. The following step could be either Tafel reaction or a Heyrovsky reaction. In Tafel reaction, two  $H_{ad}$  on the cathode react and a hydrogen molecule is formed.



In Heyrovsky reaction, a proton and an electron react directly with an adsorbed hydrogen atom and form hydrogen molecules.



The reaction path isn't always regular and predictable for HER reactions, but the HER mechanism could be generalized from the Tafel plots derived from the polarization curve. One crucial parameter that represents the experimental results of the Tafel plots is the Tafel slope. The slope shows the overall performance of the reaction, and also helps interpret the HER mechanism at active sites. There are three important values of Tafel slope that leads to the characterization of which mechanism pathway the reaction is. It is widely accepted that Tafel slopes of 120, 40 and 30mVdec<sup>-1</sup> were examined for the Volmer, Heyrovsky and Tafel determining steps. However, the value of Tafel slope can be affected by many other factors such as applied potential or mass transport in porous structure.

## 2.2 Photoelectrochemical Cells (PEC)

Developing clean energy source is undoubtedly important in an era which fossil fuels are causing global warming and gradually becoming scarce on earth. Hydrogen appears to be one of the answers to the upcoming energy issue. However, the ratio of hydrogen in the atmosphere is even lower than noble gases that are values as high scarcities due to its low density, allowing hydrogen to escape from gravity. As a result, hydrogen mainly exists in the form of compounds such as water and hydrocarbons on earth. Therefore, the methods that separate hydrogen from these compounds appears in numerous researches over decades. Water-splitting with photoelectrochemical (PEC) cells is one of the most popular techniques among all.

PEC cells could be categorized into photovoltaic cells and photoelectrolytic cells. Photovoltaic cells convert the energy of electromagnetic radiation, which is often sun light, directly into electricity by photovoltaic effect. On the other hand, photoelectrolytic cells uses the energy absorbed from the incident light to electrolyze water into oxygen and hydrogen. That is, the photovoltaic cells convert solar energy into electricity for direct use while photoelectrolytic cells store the solar energy by converting them into fuel such as hydrogen.

Water-splitting PEC cells are photoelectrolytic cells that generate hydrogen. The structure of a PEC cell is shown below in Figure 1. The cell is composed of a semiconductor anode and usually a metallic cathode in an aqueous electrolyte solution. The reaction takes place on the Schottky junction composed of semiconductors and the electrolyte at the interface. The electrode made of semiconducting material is referred as the photoanode which absorbs light.

Charge carriers, holes in the case, are formed when the light is absorbed by the photoanode. If the band gap of the semiconductor distribution of the semiconductor overlaps the band gap of  $\text{H}_2\text{O}$ , the holes generated would contribute to the water splitting process forming oxygen and  $\text{H}^+$ . The minimum band gap should be larger than 1.23V vs NHE for material selection of water splitting. The reason would be discussed in the next section.

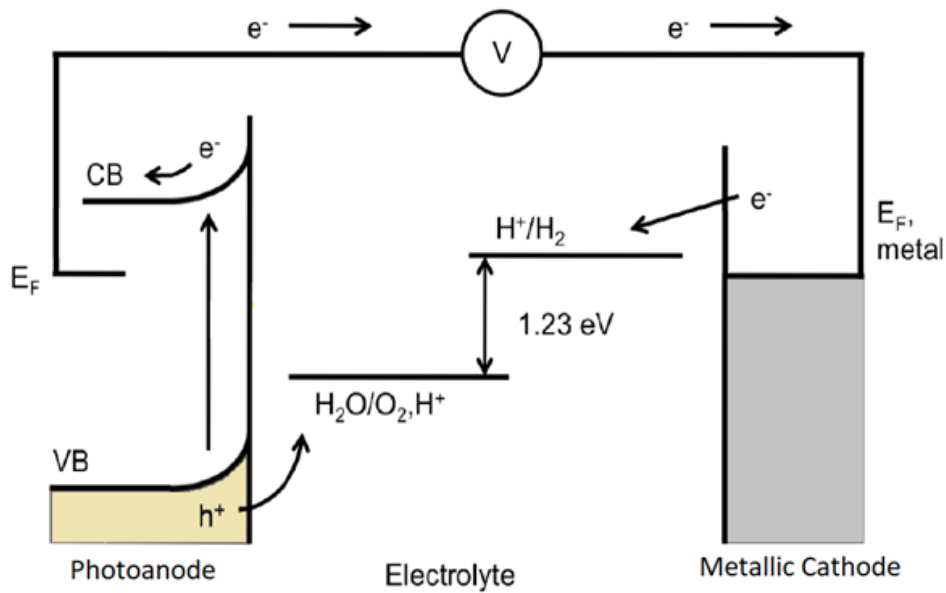


Figure 1 Structure of a PEC cell

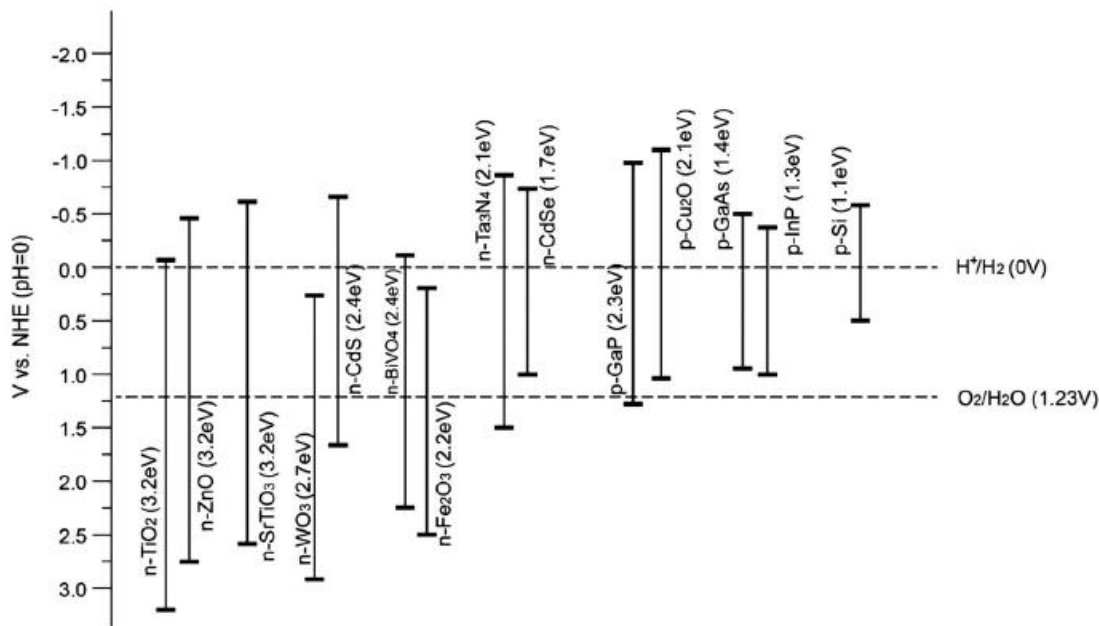
### 2.3 Material Requirements for Photoanodes

Numerous types of semiconductor materials have been used and tested for fabrication of photoanodes. Metal oxide semiconductors have drawn most attention because of their chemical stability, wide band gap, favored band edge distribution, low cost

and tunable band gaps. [5] Oxide materials is considered to be one of the most stable form of metal compound in nature while being able to be synthesized through various methods. Several oxide semiconductors are used in application of photoanodes, this section shows the criteria of materials for photoanodes and t

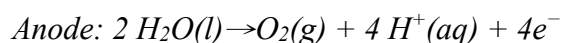
### **2.3.1 Energy Band Theory**

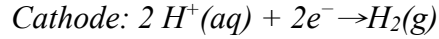
Photo energy highly depends on the wavelength, and the most desirable light is visible light. Sunlight is composed of approximately 55% infrared, 42% visible light and 3% ultraviolet. Though infrared is more than half the ratio, but the photoenergy is too low to drive photoelectrochemical reactions. On the other hand, ultraviolet is superior in energy, but the ratio is too low to be considered, making visible light the best choice of all. Visible light has the wave length rough between 380nm and 700nm, with corresponding photo energy 3.2eV to 1.8eV. This energy also sets the criterion of material selection at their band gap. The efficiency of a PEC cell is highly dependent on the selection of semiconducting material. The band gap distribution of common semiconductors is shown in Figure 2. The numbers are based on the potential where the redox reactions occur with a Normal Hydrogen Electrode (NHE) being the reference electrode. The band gap of a semiconductor should be at least larger than the band gap of water (1.23eV) for water splitting. Not only the band gap value matters, but also the band gap distribution. The reason that the band gap distribution is crucial to water splitting reaction is about driving force. In order to make the charge get involved with the redox reactions, a driving force is required.



**Figure 2 Band distribution of common semiconductors**

When the semiconductor and the aqueous electrolyte solution meet at the interface, the energy diagram changes, followed by the alignment of fermi energy levels, and finally creates band bending. The band bending is significantly related to the main driving force for charge transportation at the interface. If the conduction band of a semiconductor is positioned higher than 0V vs. NHE, the conduction band is capable of contributing electrons to generate hydrogen and O<sup>2-</sup>. On the other hand, if the valence band is positioned lower than 1.23V vs. NHE, the valence band donates holes to generate oxygen and H<sup>+</sup>. When the charge carrier reaches the solid/liquid interface, it reacts with a water molecule. The half reactions are given as the formulas below:





The first half reaction at the anode is oxidation, and it involves holes contributed by the photoanode generating oxygen; while the second half reaction at the cathode being the reduction, and involves electrons provided by the metallic counter electrode generating hydrogen. The insight for the HER reactions was mentioned earlier.

As a result, the materials of selection should have a band gap larger than 1.23V and a distribution which overlays the  $H^+/H_2$  region and the  $O_2/H_2O$  region.

### **2.3.2 Catalytic Activity and Stability**

The PEC cell is a very reliable tool for water splitting where semiconductors are used to harvest solar energy. The structure of the PEC cells shows that the reaction relies on external applied bias and the composition of the electrolyte. When the reaction of the PEC cells takes place, the faster the reaction at the surface is, the less likely to have charge accumulation. Charge accumulation leads to charge recombination and further decreases the photocurrent. Meanwhile, PEC materials must be inert and stable under reaction conditions to avoid the photocatalyst itself being decomposed during the process. The self-decomposing process is defined as photocorrosion. Photocorrosion depends upon the relative positions of the material band edges and the respective decomposition potential.

It is well known that charges are generated from the conduction band and valence band respectively under well matched illumination. Both kinds of charges may lead to charge accumulation and the self-degradation of semiconductor materials. Take photogenerated holes for example. The generated electrons are transferred to the surface while the transfer of holes becomes an issue and results in charge accumulation. The

accumulation of holes not only causes charge recombination that decreases photocurrent, but also drives the decomposition of the photocatalyst material. The consequence of this behavior is the formation of metal oxide on the surface. Resulting in further decrease in the overall performance of the photoanode.

### 2.3.3 Charge Carrier Mobility

When a charge carrier is generated by the photoanode, the charge carrier mobility of the semiconducting material would have straight impact to whether the charge carrier could travel to the solid/liquid interface to contribute to water splitting. If the charge carrier mobility is low, the distance traveled by the carrier may not be enough before charge recombination happens. In other words, if the charge recombination rate is high, the efficiency of the photoanode absorbing light, generate charge carriers for water splitting would be low because less charge made its way to get involved in the reaction.

<b>Material ⇒ Property ↓</b>	<b>Si</b>	<b>Ge</b>	<b>GaAs</b>	<b>InAs</b>	<b>InSb</b>
<b>Electron mobility</b>	<b>1600</b>	<b>3900</b>	<b>9200</b>	<b>40000</b>	<b>77000</b>
<b>Hole mobility</b>	<b>430</b>	<b>1900</b>	<b>400</b>	<b>500</b>	<b>850</b>
<b>Bandgap (eV)</b>	<b>1.12</b>	<b>0.66</b>	<b>1.424</b>	<b>0.36</b>	<b>0.17</b>
<b>Dielectric constant</b>	<b>11.8</b>	<b>16</b>	<b>12.4</b>	<b>14.8</b>	<b>17.7</b>

Figure 3 Carrier mobility of common semiconductors

Electrons move in the conduction band while holes move in the valance band. In general, the mobility of holes is lower than the mobility of electrons because the restriction of movement is different as shown in Figure 3. Both electrons and holes move under the effect of an electric field, but the electrons are located at the outer shells that are less bonded by the nucleus while holes are created by the elevation of electrons from the inner most shells to outer shells.

By definition, the charge mobility is dependent on the drift velocity, and the main factor determining the drift velocity is the scattering time. That is, how long the carrier is accelerated by the applied electric field before colliding into anything that affects its direction or energy. There are multiple factors and conditions where scattering may occur, for instance, amorphous semiconductors have much less mobility than what they are in crystalline forms because the electrons are scattered very frequently in the amorphous materials.

Summing up, the carrier mobility of a material has huge impact to the photoelectrochemical applications, it determines the diffusion length which is highly related to the thickness of the films.

## **2.4 Bismuth Vanadate**

### **2.4.1 Properties of Bismuth Vanadate**

$\text{BiVO}_4$  is a n-type semiconductor with high stability and great optical property. The band gap of  $\text{BiVO}_4$  is 2.4eV, and the distribution is shown in Figure. 2. The properties meet

the requirements listed above which is having a band gap larger than 1.23eV and a distribution which overlays the  $H^+/H_2$  region and the  $O_2/H_2O$  region.

In addition, the catalytic activity and stability of the material are important requirements of an outstanding photoanode material. The chemical stability may cause problem when the reaction is under acidic or alkaline environment. And the photocorrosion is notably promoted by applied bias and light illumination. But due to the superb band gap and the band distribution of  $BiVO_4$ , researchers have developed several strategies to solve this issue. For instance, adapting an external passivation layer on the photoanode to avoid direct contact with the electrolyte. In the case which photocorrosion occurs, the electrolyte serves as a donor or acceptor of the atoms. However, in this case, an inert layer is coated on the photoelectrode, making the photoelectrode not in direct contact with the electrolyte. As a result, even though carriers are available, photocorrosion won't occur. Other methods such as saturating the buffer electrolyte to suppress dissolution are also developed.

Aside from a superior band gap property and the chemical stability,  $BiVO_4$  has a relatively poor electronic property. The diffusion length is defined is the average distance a minority carrier moves before recombining. The importance of diffusion length in terms of photoelectric catalyst is the carrier must be eligible to move from where it was generated to where it could be collected. In other words, the longer the diffusion length is, the larger the solar cell current is.

In general, the diffusion length of semiconductors is measured with  $\mu m$ . For instance, the diffusion length in silicon is 100~300  $\mu m$ . GaAs (p-type) has a diffusion length around 200~800  $\mu m$ . [6] On the other hand, the diffusion length of pure  $SiO_2$  is

around 1.2nm. Proving SiO<sub>2</sub> a poor material for carrier diffusion. Thus, diffusion lengths at the level of nm are considered relatively small.

Diffusion length is a crucial property of PEC materials because it means the average distance carriers can travel before recombining. This property is highly related to the collection probability. Therefore, the longer the diffusion distance is, the higher chance the carrier generated by photo absorption being collected by the junction and contribute to the photo-current. However, the carrier diffusion length of BiVO<sub>4</sub> is in the range of 10nm and 70nm, which is relatively short while TiO<sub>2</sub> has a diffusion length up to hundreds of  $\mu\text{m}$ . This could be solved by various ways. For example, doping metals or non-metals to enhance charge separation and increase the diffusion length up to 300nm. [7] Recently, studies about increasing carrier mobility through pulsed laser deposition by controlling growth orientation have been conducted. This brings a new point of view of enhancing the properties of BiVO<sub>4</sub>.

To sum up, BiVO<sub>4</sub> has a band gap energy of 2.4eV and a well-matched band distribution with water splitting. BiVO<sub>4</sub> photoanodes are active under the illumination of nearly half the solar emission, and theoretically giving 9.1% STH efficiency with a maximum photocurrent density of 7.5mA/cm<sup>2</sup> under air mass (AM) 1.5 standard test conditions. [8] Air mass is defined as the ratio of incident beam path length through the atmosphere and the path length at zenith. Though the efficiency of BiVO<sub>4</sub> is encumbered by its diffusion length and its stability under acidic and alkaline environment, BiVO<sub>4</sub> is still a strong candidate in terms of materials selection for photoanodes. This thesis will focus on enhancing the carrier mobility of BiVO<sub>4</sub> through growth control.

## 2.4.2 Synthesis of Bismuth Vanadate

There are several known methods to grow  $\text{BiVO}_4$  films. For instance, chemical bath deposition was used to deposit  $\text{BiVO}_4$  in 2002. A milky suspension is formed by preparing solutions of bismuth source with EDTA and adding vanadium source sequentially. The final suspension has a ratio of 1:2:2 with  $\text{Bi}^{3+}/\text{EDTA}/\text{VO}_3^-$ . Heating the suspension with vigorous stirring would result in a clear solution in which a glass substrate is dipped in vertically and stay still under required temperature for certain amount of time. [9] People also deposit  $\text{BiVO}_4$  with sol-gel technique. The technique requires making a sol-gel solution which is based on bismuth nitrate and vanadyl acetylacetonate mixed with acetic acid and acetylacetone. The pH value of the solution is controlled to ensure the oxidation states for bismuth and vanadium to form  $\text{BiVO}_4$ . The film is fabricated by dip coating this sol-gel solution onto substrates and followed by annealing under certain temperatures. [10]  $\text{BiVO}_4$  films is also deposited through sputtering. The substrate is placed in the chamber after cleaning with ethanol and acetone. Then the film is deposited through sputtering of a  $\text{BiVO}_4$  target under certain pressure. Annealing was performed under  $500^\circ\text{C}$  after sputtering for 2 hours. [11]

There are certain advantages of the methods mentioned above. To begin with, the chemical bath deposition method is low cost, easy set-up and stable and also results in uniform films. The sol-gel technique is the simplest method with low cost and high reproducibility, the films deposited by sol-gel technique obtains good homogeneity. When it comes to sputtering, the greatest advantage is that sputtering has large area coverage. Which makes it capable of fabricating large size films. However, there are certain

drawbacks of the techniques. The chemical bath deposition (CBD) wastes a lot of the solution and the requirement of the substrate's cleanliness is high. The sol-gel method requires long periods of deposition and it is difficult to make a thick layer on the substrate. As for sputtering, the stoichiometry of oxide targets become complicated to control. Thus, pulsed laser deposition is applied to deposition of BiVO<sub>4</sub> films.

## **2.5 Crystallographic Orientation**

The physical property of a crystal is highly dependent on its crystallographic orientation. In other words, the optical, thermal, electrical and mechanical behaviors of a crystal are also determined by the crystal structures.

It has been reported that BiVO<sub>4</sub> films with preferred orientation shows better results in photoelectrochemical characterization tests. Preferred orientation is the phenomenon that grains are showing stronger tendency to be oriented toward certain crystallographic directions. Unlike powder X-ray diffraction sample preparation, we would like to see preferred orientation demonstrated by the samples to show that the crystallographic orientation is affected by the change in deposition temperature.

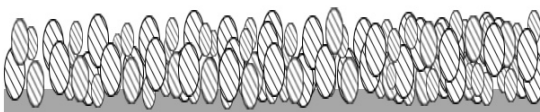
Random Orientation



Random Orientation-XRD



Preferred Orientation



Preferred Orientation-XRD



**Figure 4 Random orientation vs. preferred orientation**

As shown above in Figure 4, the XRD pattern of the sample with preferred orientation would have certain lattice planes being detected more than others, resulting in the ratio of peak intensities being intermingled.

The general method to determine if the sample is demonstrating crystallographic orientation towards certain direction It has been reported that crystallographic orientations could be controlled through several variables during the crystal growth such as temperature, pressure, the composition of precursor and the substrate surface condition. [12] This thesis will focus on controlling the deposition temperature to adjust crystallographic orientation for photoelectrochemical applications.

## 2.6 Pulsed Laser Deposition (PLD)

### 2.6.1 Introduction for PLD

Pulsed laser deposition has been widely applied over the decades and is used in a variety of thin film research fields. As the width of research widens, the material selection becomes numerous. Some materials could be processed well through other techniques such as sputtering. However, the role of PLD for depositing complex metal oxide become significant when it comes to requirements of high stoichiometry of the target material and the film deposited. The major advantage of PLD origins from the material removal mechanism. The energized photon interacts with the surface of the target and creates a plume with similar stoichiometry to the target through superheating. In comparison, the composition of the vapor created through thermal evaporation could be different since it depends on the vapor pressures of the elements of the target material.

Among the numerous thin film materials, the stoichiometry of materials with the element oxygen are more complicated to control. Take sputtering  $\text{BiVO}_4$  as an example. Sputtering has the advantage of depositing large area films. Meanwhile, the stoichiometry of oxygen is an issue in sputtering and is widely studied. On the other hand, the oxygen pressure could be set at a certain value so that the oxidation is relatively more straightforward and stable. [13]

## 2.6.2 Basic Concept of PLD

The PLD uses pulsed laser to induce the stoichiometric transfer of a material from the target to the substrate. The basic structure of PLD is show below as Figure 5 [14]. The target and the substrate are positioned parallelly inside the deposition chamber. The chamber is basically vacuum in most cases of PLD depositions which the targets are non-oxide materials. In depositions of metal oxide films, oxygen gas is infused and set at desired pressure to control the oxygen stoichiometry. A high intensity laser is generated outside the chamber and emitted into the deposition chamber through several lens controlling the size and shape of the light spot. The target material is hence evaporated by the induction of high energy photons with no contamination.

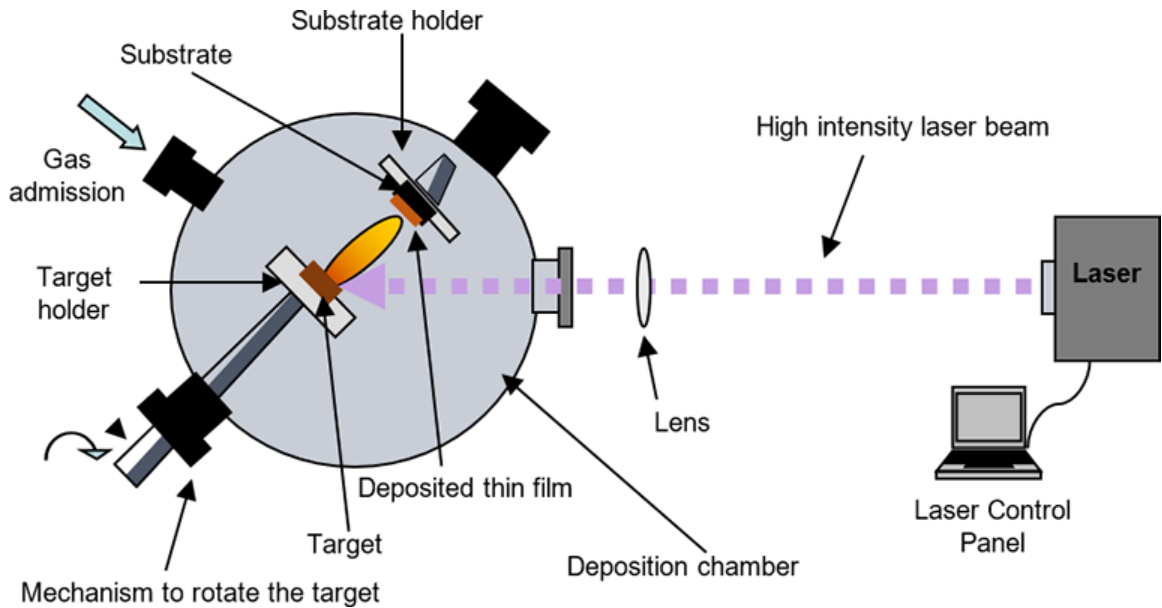


Figure 5 Experimental setup of a PLD system [14]

Though the experimental set-up sounds very simple, the complexity of the laser-material interaction is much higher and involves several processes.

First, we have to match the optical energy to the target material. [15] For each pulse, starting from the ablation, the surface of the target is heated up and melted by the incident laser. The heating rate of the PLD could be as high as  $10^{11}$  K/s. The upper layer of the molten surface evaporates and forms a plasma plume. The photons not only interact with the surface of the target, but also absorbed by the evaporated species. Consequently, the propagation of the plume in the direction normal to the target. Finally, the process returns to the initial state after a very short period of time in the scale of nanoseconds at the end of the pulse with a resolidified surface. Meanwhile, nucleation and growth take place at the surface of the substrate.

In the phase of ablation, the photons are converted into electronic excitations and then into thermal, chemical, and mechanical energy. As a result, the material at the surface is rapidly removed from the target. Since the removal of the material is fast, a mirror raster has to be set along with the rotation of the target to maximize usage of the whole target and avoid burning all the way through. The laser fluence at the surface of the target is required to exceed a threshold ranging from 1 to 3 J/cm<sup>2</sup> for a typical KrF excimer laser.

Factors that are responsible for PLD deposition include deposition conditions, laser beam parameters, and the material property of the target. [14] Vacuum status, reactive gas pressure, throwing distance and number of pulses per second are known as deposition conditions. The wave length and the pulse duration fluence defines the laser beam parameters. Last, the melting temperature, thermal diffusion rate and optical reflectivity are main material properties for the target.

### **2.6.3 Influence of Deposition Condition**

When the target material is selected, the variables of the deposition mainly sit in the category of deposition condition. Depending on the structure and thickness of one's desire, the film could be totally different under different deposition conditions.

The substrate temperature of the substrate is a very important parameter that could be easily adjusted with PLD. During deposition of the film, there are several physical processes taking place on the surface of the substrate. Materials removed from the target forms the plume and hits the substrate. The interaction between those particles is highly influenced by the substrate temperature. [16] The substrate temperature determines the activation energy of the plume particles and the atom mobility on the substrate surface. This thesis mainly focuses on the impact of substrate temperature to the performance of BiVO<sub>4</sub> films deposited with PLD.

## **3.0 Research Description**

### **3.1 Hypothesis**

The hypothesis of this study is that the overall performance of photoelectrochemical performance of BiVO<sub>4</sub> films could be enhanced when the crystallinity is increased.

### **3.2 Objectives**

The objective of this study is to enhance the crystallinity of BiVO<sub>4</sub> films with PLD by controlling the deposition condition. By examining the effect of deposition temperature on the BiVO<sub>4</sub> film properties fabricated with PLD, we will be able to tell the influence of temperature by comparing the SEM images, X-Ray diffraction patterns data and the PEC performances of films deposited under different temperatures. Influence of thickness on film performance is also planned.

### 3.3 Research Tasks

The first task of this thesis is to coat  $\text{BiVO}_4$  films on FTO substrates under various deposition conditions and anneal the samples. The second task is to measure the thickness of the films to ensure the deposition rate and condition is as expected. The third task is to collect the SEM and XRD data. The microstructure of the films could be characterized and result in showing the influence of certain variables adjusted during the deposition process. Last, we characterize the PEC performance by measuring the J-V curve of the films under simulated solar illumination and compare the results to traditional  $\text{BiVO}_4$  films.

## 4.0 Experimental Section

### 4.1 Synthesis of BiVO<sub>4</sub> Films with PLD

A BiVO<sub>4</sub> target (PVD Products) for pulsed laser deposition is used for the deposition of BiVO<sub>4</sub> films done with the pulsed laser deposition system (PVD Products). The pulse energy is set at 150mJ, making the energy density around 3 J/cm<sup>2</sup>. The frequency of the laser pulse varies from 10Hz to 40Hz. The deposition time length from 20 minutes to 4 hours, resulting in the overall thickness being controlled between 1 micrometer and 200nm. The oxygen pressure was set at 10mtorr for all depositions. The deposition temperature ranges from room temperature to 600C. For high temperature depositions, the substrate was preheated for 20 minutes to ensure the temperature of the substrate matches the desired temperature. The distance between the target and the substrate is controlled at 60mm, this is also defined as the throwing distance. The BiVO<sub>4</sub> films were annealed at 500 °C for 1 hour after deposition.

Three samples are made per batch with different positions relative to the center of the substrate holder. The plume of the PLD should have the highest density at the center and decrease gradually to the edge of the round substrate resulting in change of thickness.

## 4.2 Microstructural Characterization

After synthesis, the microstructure of  $\text{BiVO}_4$  films were characterized with SEM (SEM FEI, Apreo) and XRD (D8 XRD System, Bruker).

The scan range of the XRD was from 10 to 60 degrees (2 theta), with an increment of 0.02 degrees at the speed of 0.5 seconds/step, resulting in a scan time of 20 minutes. The morphological trait of the films was characterized with by the SEM at a magnification of 35000x.

## 4.3 Electrochemical Characterization

Electrochemical properties of  $\text{BiVO}_4$  samples were measured in a proper electrolyte for each composition at constant temperature using amperometry technique conducted in a three-electrode system shown in Figure 6. Amperometry generally refers to all electrochemical techniques in which a current is measured as a function of either time (potentiostatic amperometry) or applied electrode potential (voltammetry). In this research, we perform potentiostatic amperometry where current is measured at a constant potential with variation of the deposition time for nanowire coating. An electrochemical station (CH Instruments) is used is connected to an FTO/glass substrate as the working electrode and a platinum wire as a counter electrode, with the potential kept fixed with respect to an Ag/AgCl reference electrode (Accumet, Fisher Scientific). The electrolyte is an aqueous 0.5 M potassium phosphate buffer, using  $\text{KH}_2\text{PO}_4$  (Sigma-Aldrich, Reagent grade, 1.0 M)

solution and  $K_2HPO_4$  solution (Sigma-Aldrich, Sigma-Aldrich, Reagent plus, 1.0 M) buffered to  $pH \approx 7 \pm 0.02$ .

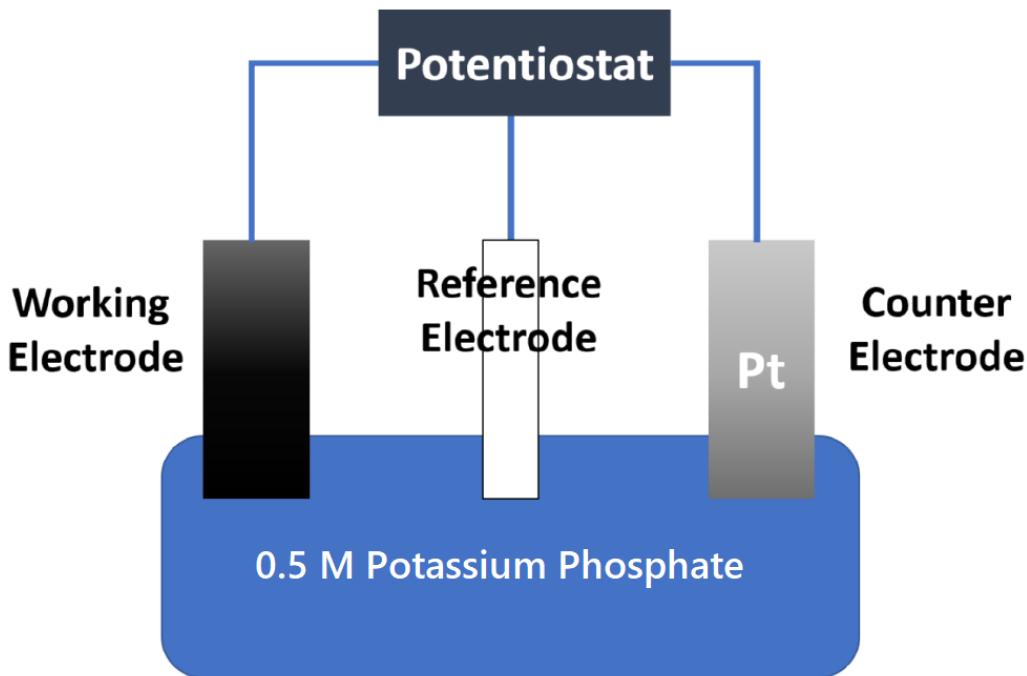


**Figure 6 Electrode setup for photoelectrochemical measurements.**

We performed potentiostatic amperometry (LSV) to the photoanode to characterize the performance under illumination. The current measured at the potential of 1.23V vs RHE is defined as the value of photocurrent which we are interested in. In LSV measurement, we set the potential range from -0.5 V to +2.0 V to measure the photocurrent of the working electrode. The scan rate of the potential is set at 100mV/s controlled by the electrochemical workstation. The potential vs Ag/AgCl were converted to the reversible hydrogen electrode (RHE) using the Nernst Equation below.

$$E(RHE) = E(Ag/AgCl) + E^0(Ag/AgCl \text{ vs NHE}) + 0.059pH$$

$$\text{where } E^0(Ag/AgCl \text{ vs NHE}) = 0.207 \text{ V at } 25^\circ\text{C}$$

The BiVO<sub>4</sub> photoanode is measured under simulated AM 1.5 solar illumination (100mA/cm<sup>2</sup>) with a Newport Solar Simulator using appropriate filters and calibrated using Si photodiode. The working area of the photoanode being illuminated is 0.28 cm<sup>2</sup>.

## 5.0 Experimental Results and Discussion

In this section, data including film thickness, SEM images, XRD plots and LSV curves are shown to explain the effect of deposition conditions to the properties of the films.

### 5.1 Thickness Control of BiVO<sub>4</sub> Films

The properties of the films are highly dependent on the film thickness. On one hand, the film has to be thick enough to absorb light instead of letting light go through. On the other hand, the film also has to be thin enough due to the limitations of carrier mobility as mentioned in section 2. The variables of the deposition conditions are listed as oxygen partial pressure, throwing distance, repetition rate and deposition time.

The thickness is also affected by the position of the substrate because of the shape of the plume. Different positions on the substrate holder results in different deposition rate due to the shape of the plume. The thickness of the films deposited at the center is approximately 1.2 times thickness of films deposited 1.5cm off center, and 1.5 to 2 times thickness of films 3cm off center.

### 5.1.1 Growth Behavior as a function of Oxygen Partial Pressure

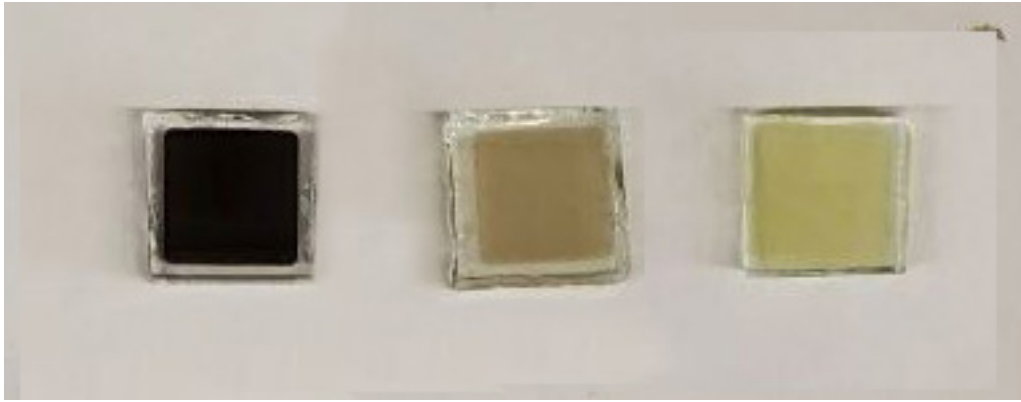
The plume is also highly affected by the gas pressure, we would like to determine the optimal oxygen partial pressure. The chamber is pumped down to  $10^{-4}$  mtorr in advance, and the films are deposited at room temperature with a throwing distance of 85mm of position 1 under various oxygen partial pressure for 30 minutes. The results are shown as below in Table 1.

**Table 1 Film thickness and appearance under different oxygen partial pressure**

	Color	Thickness
150mtorr	Transparent	-
50mtorr	Transparent	-
20mtorr	Yellow-Transparent	23nm
10mtorr	Yellow-Brown	78nm
5mtorr	Brown-Black	72nm
No Oxygen	Black-Brown	81nm

Although oxygen is highly required in the deposition of  $\text{BiVO}_4$  films, the thickness drops dramatically under pressure higher than 10 mtorr. The possible reason for this drop is the loss of kinetic energy under higher oxygen partial pressure. The materials in the plume lost kinetic energy because of collision taking place with oxygen. Due to the fact that thickness is required for optical absorbance, the film should be thicker than 200 nm or the incident photons would not be collected by the photoanode. We tested samples with thickness within 200nm which is not listed in this study. However, the film was too thin that the photocurrent is below one tenth the results reported in this thesis. Meanwhile, the

color of the films should not be opaque and dark because that implies that vacancies for oxygen and lots of defects are formed inside the film. Needless to mention that a film with numerous defects wouldn't perform well from all perspectives. The lack of oxygen could also ruin the stoichiometry of the  $\text{BiVO}_4$  film. As a result, taking both thickness and appearance into consideration, an oxygen partial pressure of 10mtorr is chosen for the



depositions.

**Figure 7 Physical Appearance of films deposited under (a) No Oxygen (b) 5mtorr (c) 10 mtorr**

### **5.1.2 Thickness as a function of repetition rate and deposition time**

The repetition rate and deposition time determines the total pulses of the PLD deposition. Theoretically, the thickness of the film deposited per pulse would be the same and defined as the deposition rate ( $\text{\AA}/\text{pulse}$ ). The pulse energy is set at 150mJ for all depositions. The reference papers recommended to use a repetition rate of 10 Hz and deposit for 10 to 60 minutes resulting in a deposition rate around 0.3~0.5  $\text{\AA}/\text{pulse}$ . The initial deposition rate for our system was 0.01  $\text{\AA}/\text{pulse}$  for the sample at the center, which

was far off the data from references. The reason for the condition is the loss of pulse energy due to contamination of laser gas which resulted in losing nearly half of the deposition rate. In addition, changing the throwing distance from 85mm to 60mm also doubled the film thickness, so the throwing distance is set at 60mm. With an adjustment and calibration of the mirror raster of the PLD, the deposition rate is increased to around 0.12 Å/pulse. After depositing the films with different thicknesses ranging from 200 nm to 1200 nm. We test the photoelectrochemical performance of the films and adjust our deposition condition for the next depositions, resulting in a chart showing the results of depositions under different deposition conditions as Table 2 below.

**Table 2 Film thickness under various deposition conditions**

Condition	Position	Center	1.5cm Off	3cm Off
RT, 40Hz, 20min		582nm	460nm	231nm
500°C, 40Hz, 20min		537nm	384nm	265nm
600°C, 40Hz, 20min		513nm	369nm	223nm
RT, 40Hz, 30min		731nm	605nm	N/A
500°C, 40Hz, 30min		725nm	597nm	N/A
600°C, 40Hz, 30min		716nm	582nm	N/A
600°C, 10Hz, 60min		351nm	-	-
600°C, 10Hz, 120min		500nm	385nm	290nm
600°C, 15Hz, 120min		712nm	590nm	430nm
600°C, 15Hz, 240min		1200nm	1058nm	814nm

## **5.2 Microstructure of BiVO<sub>4</sub> Films**

The change in microstructure of the films deposited under different temperature is observed with SEM and XRD measurements.

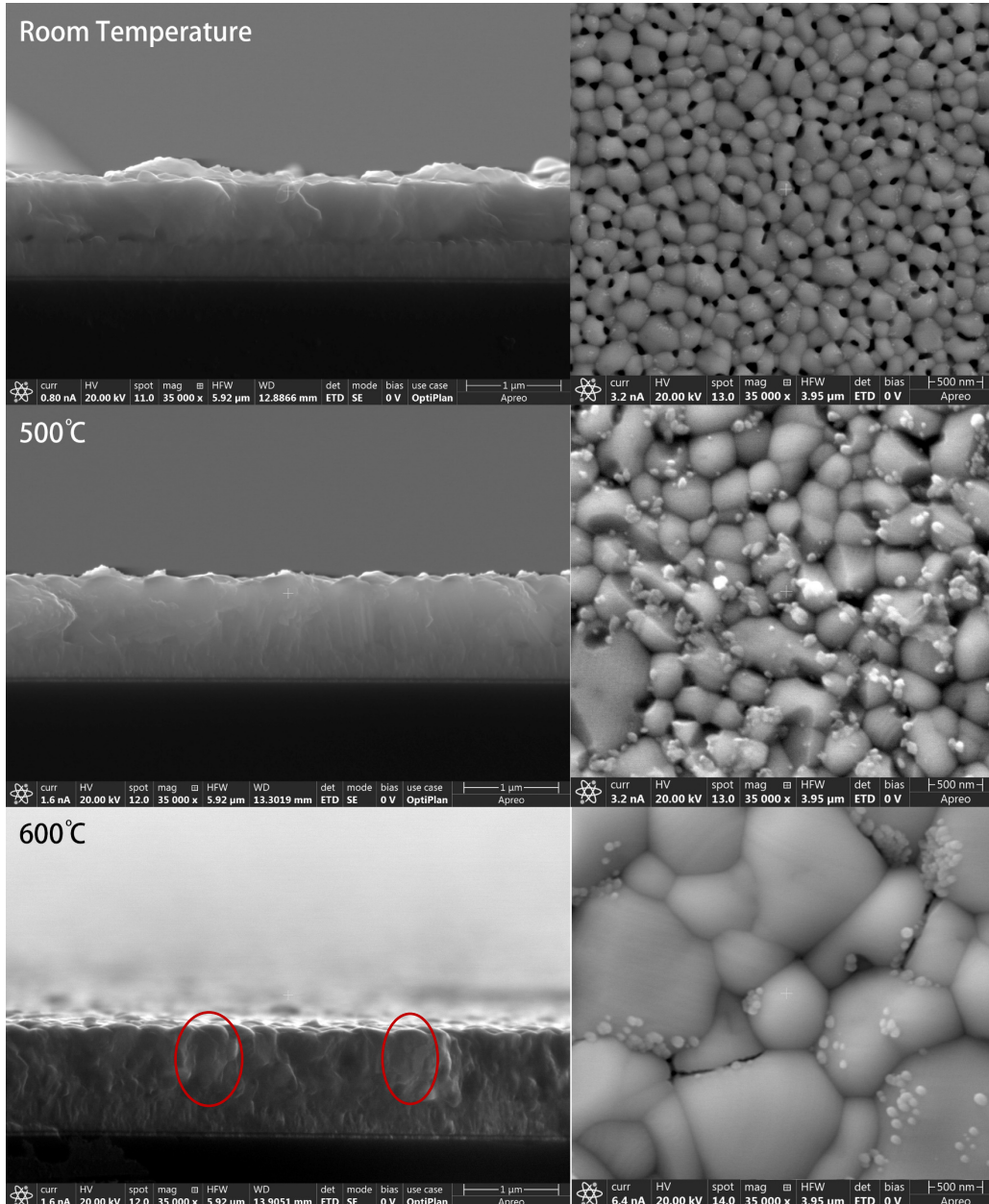


**Figure 8 SEM images of BiVO<sub>4</sub> Films**

The SEM images shows the cross-section structure on the left, and the top view of the films on the right. Increase in grain size is observed in samples of 500°C. Columnar structure is observed for 600°C samples. In addition, the grain size of the 600°C samples

exceeded the ones of 500°C. On the other hand, the film deposited under room temperature doesn't show the structure observed on the high temperature films. This indicates that the structure and size of the grains is highly related to the deposition temperature.

We have examined that the grain size and the columnar structure is determined through the SEM images, and next on we determine the orientation of the grain through XRD.

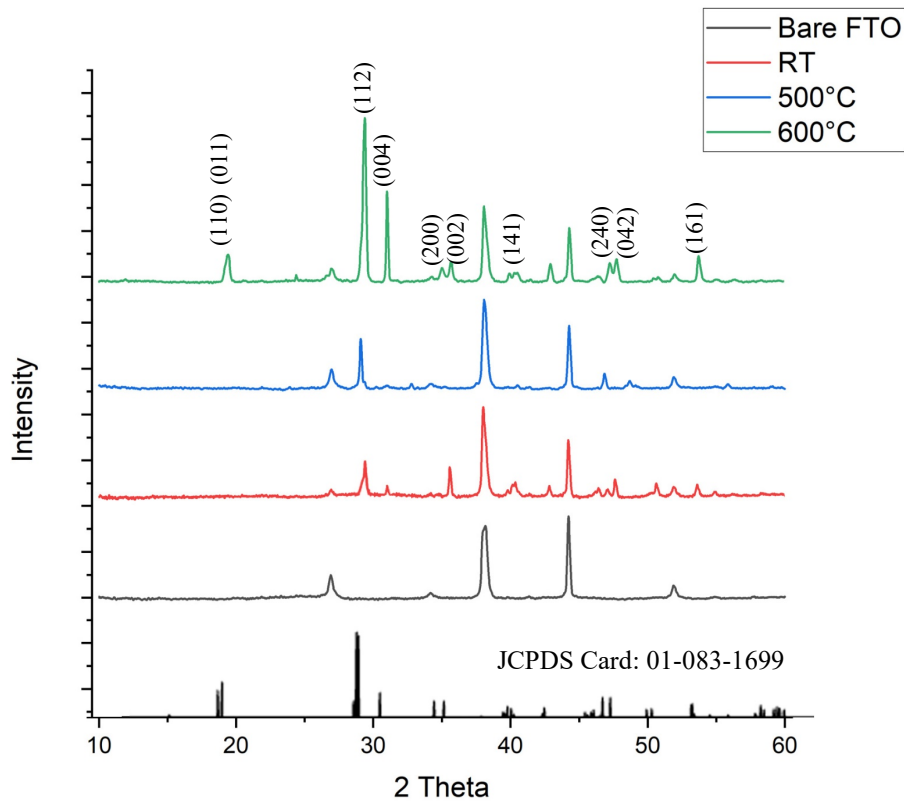


**Figure 9 XRD plots of BiVO<sub>4</sub> Films**

The BiVO<sub>4</sub> films are all deposited under the same condition with a repetition rate of 40 Hz, 30 minutes of deposition time and 10 mtorr oxygen partial pressure ending up with thicknesses around 750nm for better XRD results. As shown in Figure 9, the sample

deposited under room temperature wasn't showing sharp peaks aside from the peaks resulted from the FTO substrate. This implies that the crystallinity of the particles is low, and the grains are randomly oriented. However, the intensity of the (112) peak for 500°C increased nearly one half the intensity comparing with the room temperature sample. The intensity of the (112) and (004) peak sharply increased for the sample deposited under 600 °C while other peaks remain similar intensity comparing with the room temperature sample. This means that the samples are exhibiting higher crystallinity when deposited under higher temperatures. Also, we are observing preferred orientation under deposition at high temperatures towards [112] and [001] direction. In addition, the overall ratio of [112] and [004] oriented grains increased when the deposition temperature increases from 500°C to 600°C. In addition, the intensity of the (004) peak increased sharply comparing with the intensity of room temperature samples and the JCPDS card. We could conclude that preferred orientation towards [112] and [004] is observed at 600°C.

### **5.3 PEC Performance of BiVO<sub>4</sub> Films**

We have characterized the thickness and microstructure of the films deposited under various deposition conditions. The previous section showed that preferred orientation of BiVO<sub>4</sub> grains could be conducted by raising the deposition temperature higher than 500 °C. In this study, photoelectrochemical performance of BiVO<sub>4</sub> films deposited under different conditions shown in Table 2 is being measured in the form of current density vs. voltage (J-V) curve. The measurement is done with a three-electrode

setup consisted of a reference electrode, a working electrode and a counter electrode. The photoanodes were examined both in a dark condition and a simulated solar illumination condition (AM1.5G, 100mW/cm<sup>2</sup>).

As the applied positive potential increases, the photoanodes exhibit a steady increase of the photocurrent responses with negligible dark currents. When a positive bias is applied, the holes (minority charge carrier) are driven toward the interface of BiVO<sub>4</sub> and the electrolyte, and the electrons (majority charge carrier) are driven toward the interface of BiVO<sub>4</sub> and FTO. The holes driven toward the BiVO<sub>4</sub>/electrolyte interface participate in water oxidation reaction, and oxygen evolution reaction takes place.

### 5.3.1 Influence of Temperature to PEC Performance

In this study, first we examine the influence of deposition temperature to photoelectrochemical performance. We put the LSV curves of films deposited under similar conditions except deposition temperature together as shown below.

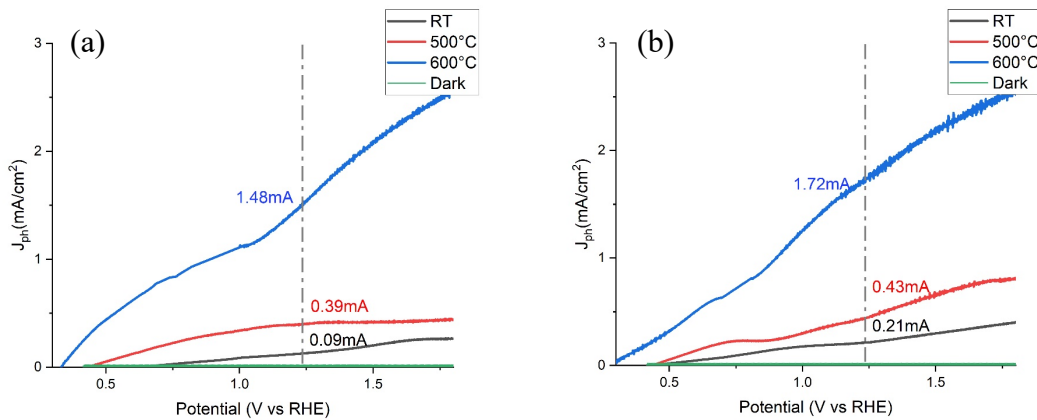


**Figure 10 J-V curves of BiVO<sub>4</sub> films with thickness of 600nm with different repetition rate. (a)40Hz , 20minutes (b) 15Hz, 120minutes**

As shown in Figure 10, the photocurrent density at 1.23V vs. RHE of films deposited at 600°C is consistently the highest. Followed by films deposited at 500°C, and the photocurrent density of films deposited under room temperature being the lowest. For (a) and (b), the thickness of the films is similar, the deposition condition, the position, and the annealing condition are all identical except for the deposition temperature. Combining the results with the XRD results reported in section 5.2, the films showing higher crystallinity and certain level of preferred orientation demonstrates better photoelectrochemical performance than the films showing random orientation. Given that randomly oriented polycrystalline BiVO<sub>4</sub> photoanodes suffer from poor charge carrier mobility, the results of this study indicates that the higher photocurrent is attributed to higher crystallinity and preferentially [112] and [001] oriented growth of BiVO<sub>4</sub>. The enhanced crystallinity and controlled growth along [112] and [001] orientation greatly improves the charge transport and suppresses electron-hole recombination.

### **5.3.2 Influence of Thickness to PEC Performance of BiVO<sub>4</sub> Films**

The previous section showed that deposition temperature and the crystallographic orientation has huge impact on the photoelectrochemical performance of BiVO<sub>4</sub> films, also implying that the carrier mobility is enhanced. Previously, the optimal thickness for traditional BiVO<sub>4</sub> films is around 230 nm. The hole diffusion length of typical BiVO<sub>4</sub> films is about 100 nm. The photogenerated holes can travel through the material to reach the interface and be separated from electrons as long as the BiVO<sub>4</sub> feature size is smaller than the diffusion length. When the thickness of typical BiVO<sub>4</sub> films becomes thicker than the diffusion length, the recombination of photogenerated charge carriers within the BiVO<sub>4</sub>

films becomes dominant, resulting in poor photoelectrochemical performances. However, the ability to absorb light of a film with thickness of 230 nm is low since the film is a little transparent. In order to secure enough light absorption, the thickness of the BiVO<sub>4</sub> films has to be increased. In this section, we would measure the J-V curves of films deposited under 600°C with thicknesses ranging from 200nm to 1200nm to see the behaviors as shown below. Photocurrent density at 1.23V vs. RHE is being recorded with corresponding thickness data.

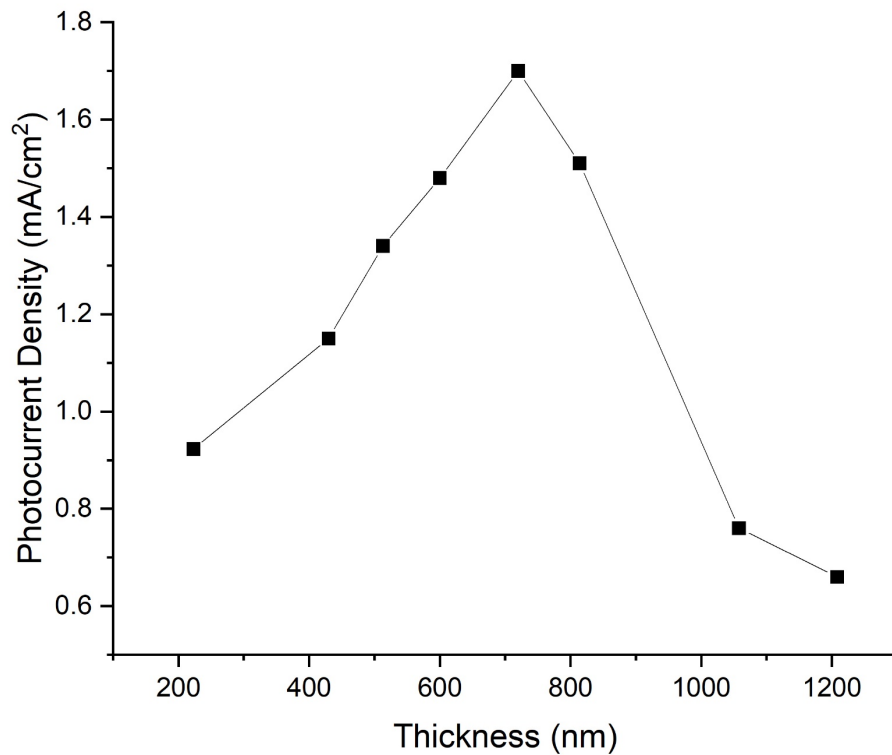


**Figure 11 Photocurrent density of 600°C deposited BiVO<sub>4</sub> Films with various thickness**

Figure 11 shows that the highest photocurrent measured is at the thickness of 720nm with photocurrent density of 1.7mA/cm<sup>2</sup>. The optimal thickness in this study exceeded the optimal thickness of BiVO<sub>4</sub> films reported previously by nearly four times.

There is a dramatic current drop for films thicker than 1 micrometer. This result indicates that the charge transport efficiency is highly improved through controlling grain growth under high temperature deposition, but it still has limitations when the film thickness becomes too large.

#### **5.4 Future Work**

Photoelectrochemical reaction of a photoanode is sensitive to its microstructure and crystallographic orientations. The structure of the film is highly dependent on the synthesis method. In this study, pulsed laser deposition (PLD) is applied to synthesize the  $\text{BiVO}_4$  films and the structure is characterized with SEM and XRD.

The properties of the films are not fully characterized yet. For instance, the optical properties could be examined more detailed in terms of transmittance and absorbance of the samples as a function of thickness and temperature. In addition, the electrical properties for the film deposited are not completely examined. With the usage of conductive AFM, the conductivity could also be mapped as a function of location. We will be able to get a more insightful view of the electrical behaviors of grains and grain boundaries of samples prepared under different conditions. Also, the film uniformity could also be examined to ensure that the film is uniform and well deposited. The conductivity also helps examine if

the films are in good condition and could eliminate certain errors caused by individual difference of samples affecting the overall performance of the photoanode.

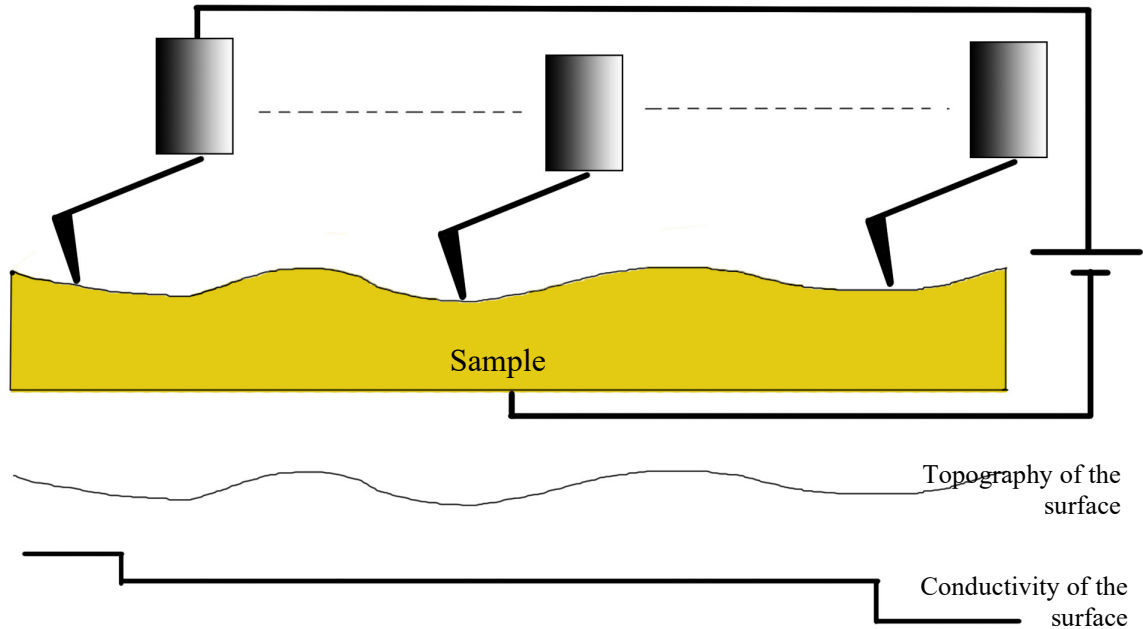


**Figure 12 Schematic diagram of conductive AFM system**

The AFM could also give an understanding of the relationship between thickness and conductivity as shown in Figure 12, bringing more insightful examination to the properties of the  $\text{BiVO}_4$  films.

In addition to the properties of the  $\text{BiVO}_4$  films, there is also space of improvement of controlling the orientation. As shown in Figure 9 in section 5.2, the grain growth orientation began to show certain preferred direction under deposition at higher temperatures. The intensity of the (112) peak starts to increase at  $500^\circ\text{C}$  and became dominant at  $600^\circ\text{C}$ . The PEC measurements also show that preferred orientation helps improving the charge carrier transport efficiency. One thing to be mentioned is that the

FTO substrate and the monoclinic BiVO<sub>4</sub> has similar structure at certain planes shown below.

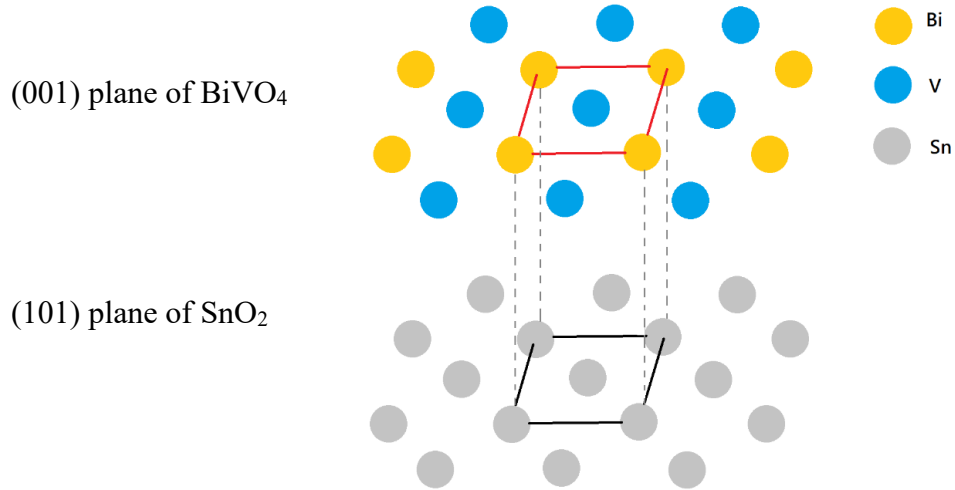


**Figure 13 The expected atomic arrangement at the interface**

Figure 13 shows the structure of BiVO<sub>4</sub> and FTO could be similar at certain planes. The XRD data also showed the appearance of (004) plane at 600°C. We already observed that the charge transport efficiency is enhanced with a preferred orientation towards [112] direction. Since the (101) plane of FTO and (001) plane of BiVO<sub>4</sub> have a structural similarity, it is very likely that further growth control along [001] direction could be executed. This could result in an even better outcome of enhancing the charge carrier transfer efficiency and the photocurrent density.

## 6.0 Conclusion

This study examines the effect of deposition condition to properties of films during synthesis of  $\text{BiVO}_4$  films via pulsed laser deposition. The thickness, appearance as of color, crystallographic orientation of the grains, and photoelectrochemical performance are all highly dependent on the deposition condition. The purpose of this study was to influence the crystallographic orientation through controlling the deposition temperature. In order to compare the results fairly under the same parameters except temperature, samples of same thicknesses, deposition rate, pulse frequency, etcetera were synthesized. By comparing the data collected through XRD, SEM, and LSV measurements, we get the conclusions as below:

For deposition done under room temperature, films have smaller grain structure with larger resulting in random orientation with a photocurrent density around 0.1mA for films of 600nm thickness. When the deposition temperature is risen to 500°C, the structure of the films starts to exhibit different peak intensities in the XRD diagram, implying that the film is demonstrating higher crystallinity and exhibiting some level of preferred orientation. In the condition of 600°C, the [112] peak and [004] peak becomes dominant in comparison to other peaks. The SEM also shows that the grain becomes more columnar as the deposition temperature rises.

The photoelectrochemical characterization measurements also show that the current density of the films increases as the deposition temperature increases. This is consistent with the conclusion of previous reference researches reporting that higher

crystallinity and preferred orientation leads to better photocurrent density because of enhanced charge carrier transfer efficiency. In addition, the thickness of the films synthesized via PLD exceeded the thickness of typical BiVO<sub>4</sub> films. This is the proof of enhanced carrier transfer efficiency.

To sum up, the higher the deposition temperature is, the more the films show preferred orientation. In this case, columnar structure starts to form and resulting in better charge mobility from FTO substrate to the surface of the film. Hence, better photoelectrochemical performance is measured comparing to films deposited under room temperature.

## Bibliography

- [1] M. Gratzel, *Nature*, 2001, 414,338.
- [2] M. G. Walter, E. L. Warren, J. R. McKone, S. W. Boettcher, Q. Mi, E. A. Santori and N. S. Lewis, *Chem. Rev.*, 2010, 110, 6446–6473.
- [3] A. J. Bard and M. A. Fox, *Acc. Chem. Res.*, 1995, 28, 141–145.
- [4] H. S. Han, S. Shin, D. H. Kim, I. J. Park, J. S. Kim, P. Huang, J. K. Lee, I. S. Cho and X. Zheng, *Energy & Environmental Science*, 2018, 5
- [5] R. Marschall, L. Wang, *Catal. Today* 2014, 225, 111.
- [6] K.S.A. Butcher, D. Alexiev, T. L. Tansley and S. Leung, *Australian Nuclear Science and Technology Organisation*, 1990
- [7] M. Huang, J. Bian, W. Xiong, C. Huang and R. Zhang, *Journal of Materials Chemistry A*, 2018, 8
- [8] L. Han, F. F. Abdi, R. Krol, R. Liu, Z. Huang, H. J. Lewerenz, B. Dam, M. Zeman and H. M. Arno, Smets, *ChemSusChem*, 2014, 7, 10, 2832-2838
- [9] M. C. Neves and T. Trindade, *Thin Solid Films*, 2002, 406, 1-2, 93-97
- [10] S. Hilliard, D. Friedrich, St. Kressman, H. Strub, V. Artero, C. Laberty-Robert, *ChemPhotoChem*, 1, 6, 273-280
- [11] S. Ju, J. Jun, S. Son, J. Park, H. Lim, W. Kim, D. Chae, and H. Lee, *ACS Sustainable Chem. Eng.* 2020, 8, 49, 17923–17932
- [12] Z. Xie, J. Bai, Y. Zhou, Y. Gao, J. Park, T. Guillemet, L. Jiang, X. Zeng and Y. Lu, *Sci Rep*, 2014, 4, 4581
- [13] Koster, G., Blank, D.H.A. and Rijnders, G.A.J.H.M., *J Supercond Nov Magn*, 2020, 33, 205-212
- [14] D. Yang, *Applications of Laser Ablation - Thin Film Deposition, Nanomaterial Synthesis and Surface Modification*, 2016
- [15] C. Belouet, *Applied Surface Science*, 1996, 96-98, 630-642
- [16] E. Hasabeldaim, O.M. Ntwaeaborwa, R.E. Kroon, E. Coetsee, H.C. Swart, *Optical Materials*, 2017, 74, 139-149

- [17] T. Saison, N. Chemin, C. Chanéac, O. Durupthy, L. Mariey, F. Maugé, V. Brezová and J. P. Jolivet, *The Journal of Physical Chemistry C*, 2015, 119, 23, 12967–12977
- [18] A. Malathi, J. Madhavan, M. Ashokkumar, P. Arunachalam, *Applied Catalysis A: General*, 2018, 555, 47-74
- [19] F. Rullens, A. Laschewsky and M. Devillers, *Chem. Mater.*, 2006, 18, 3, 771–777
- [20] V. Rajalingam, *Condensed Matter*, 2014, NNT: 2014LEMA1018
- [21] X. Yao, X. Zhao, J. Hu, H. Xie, D. Wang, X. Cao, Z. Zhang, Y. Huang, Z. Chen, T. Sritharan, *iScience*, 2019, 19, 976-985
- [22] S. Murcia-López, C. Fàbrega, D. Monllor-Satoca, M. D. Hernández-Alonso, G. Penelas-Pérez, A. Morata, J. R. Morante and T. Andreu, *ACS Appl. Mater. Interfaces*, 2016, 8, 6, 4076-4085
- [23] C. Jiang, S. J. A. Moniz, A. Wang, T. Zhang and J. Tang, *Chem. Soc. Rev.*, 2017, 46, 4645
- [24] B. Weng, M. Y. Qi, C. Han, Z. R. Tang and Y. J. Xu, *ACS Catal.*, 2019, 9, 4642-4687
- [25] H. M. Christen and G. Eres, *J Phys Condens Matter*, 2008, 20, 264005
- [26] H. Luo, A. H. Mueller, T. M. McCleskey, A. K. Burrell, E. Bauer and Q. X. Jia, *J. Phys. Chem. C*, 2008, 112, 15, 6099–6102
- [27] A. J. E. Rettie, S. Mozaffari, M. D. McDaniel, K. N. Pearson, J. G. Ekerdt, J. T. Markert and C. B. Mullins, *J. Phys. Chem. C*, 2014, 118, 46, 26543–26550
- [28] S. Khoomortezaei, H. Abdizadeh and M. R. Golobostanfard, *ACS Appl. Energy Mater.*, 2019, 2, 9, 6428–6439
- [29] J. Song, J. Cha, M. G. Lee, H. W. Jeong, S. Seo, J. A. Yoo, T. L. Kim, J. Lee, H. No, D. H. Kim, S. Y. Jeong, H. An, B. H. Lee, C. Bark, H. Park, H. W. Jang and S. Lee, *J. Mater. Chem. A*, 2017,
- [30] J. Song, K. S. Choi, M. J. Seo, Y. R. Jo, J. Lee, T. L. Kim, S. Y. Jeong, H. An, H. W. Jang, B. J. Kim, C. Jeon, and S. Lee, *Chem. Mater.*, 2018, 30, 16, 5673–5681